LLNL-JRNL-825777

LAWRENCE
LIVERMORE
NATIONAL
LABORATORY

Exploring the Effects of Emplacement Conditions on Explosion P/S Ratios Across Local to Regional Distances

M. L. Pyle, W. R. Walter

August 13, 2021

Seismological Research Letters

Exploring the Effects of Emplacement Conditions on Explosion P/S Ratios Across Local to Regional Distances

Moira L. Pyle[1] and William R. Walter[2]

[1]Corresponding Author
Lawrence Livermore National Laboratory
7000 East Ave.
Livermore, CA 94550
pyle4@llnl.gov
925-423-3820

[2]Lawrence Livermore National Laboratory
7000 East Ave.
Livermore, CA 94550
walter5@llnl.gov
925-423-8777

Prepared for submission to SRL
LLNL-JRNL-825777
Cleared for Release

Abstract

High-Frequency (~> 2 Hz) seismic P/S amplitude ratios are well-established as a discriminant to distinguish between natural earthquakes and underground explosions at regional distances (~200-1500 km). As research shifts towards identifying lower-yield events, work has begun to investigate the potential of this discriminant for use at local distances (< 200 km), where initial results raise questions about its effectiveness. Here we utilize data from several chemical explosion experiment series at the Nevada National Security Site in southern Nevada in the United States to study explosion Pg/Lg ratios across the range of local to regional distances. The experiments are conducted over differing emplacement conditions, with contrasting geologies and a variety of yields and depths of burial, including surface explosions. We first establish the similarities of Pg/Lg ratios from chemical explosions to those from historic nuclear tests and conclude that, as previous data has suggested, chemical explosion ratios are good proxies for nuclear tests. We then examine Pg/Lg ratios from the new experiment series as functions of distance, yield, depth of burial, and scaled depth of burial. At far-local and regional distances, we observe consistently higher ratios from hard rock explosions compared to ones in a weaker dry alluvium medium, consistent with prior regional distance results. No other trends with yield, depth of burial, or scaled depth of burial are strongly evident. Scatter in the observed ratios is very high, particularly at the shortest event-to-station distances, suggesting that small-scale path effects play a significant role. On average, the local distance explosion Pg/Lg ratios show remarkable consistency across all the variations in emplacement. Explosion source models will need to reproduce these results.

Introduction

One of the primary tools for discrimination between underground explosions and the natural, background seismicity is the seismic P/S amplitude ratio. Various combinations of regional P- and S-phases have been investigated (Pn/Lg, Pn/Sn, Pg/Lg), and at sufficiently high frequencies (approximately > 2-4 Hz; e.g., Kim et al., 1993; Walter et al., 1995; Taylor 1996; Hartse et al., 1997) and provided that path and structure effects have been accounted for (e.g., Taylor and Hartse, 1998; Rodgers et al., 1999; Pasyanos and Walter, 2009), this discriminant has been shown to be effective at numerous sites around the globe (e.g., Bottone et al., 2002; Rodgers and Walter, 2002; Pasyanos et al., 2014; He et al., 2018; Kim et al., 2018; Walter et al., 2018; Ma et al., 2020). Most previous studies on P/S ratios are confined to regional distances (~200-1500 km), but the ability to discriminate lower yield explosions may necessitate the use of data at local distances (< 200 km) if phase arrivals are too attenuated for amplitude measurements on regional seismograms. Some work has been done to test the extension of the P/S ratio discriminant for smaller magnitude events at shorter distances (e.g., O'Rourke et al., 2016; Pyle and Walter, 2019; Wang et al., 2020). A striking feature of these studies is the large variability in the ratio values at different local distance stations. Generally, it has been found that network-averaged ratios perform reasonably well, and Bayesian kriging shows promise for improving path corrections for single station discrimination (Wang et al., 2021), but it is not yet clear how reliable local P/S ratios are for the purposes of transportability to new regions. A better understanding of the causes of the variability in local results is necessary for confidence in their utilization.

The origin of the P/S ratio discriminant is thought to be due to the differences in source mechanism between earthquakes and explosions. The shear slip of earthquakes produces large S-waves, while the pressure pulse of an explosion should theoretically generate no shear energy.

Additionally, high-frequency shear energy that is generated by explosions is expected to attenuate more rapidly than that from earthquakes because of the depth differences typical for the events. Shallow explosions propagate more shear energy into the shallowest crustal layers with higher attenuation than earthquakes with deeper sources leading to less expected shear energy from explosions (e.g. Goldstein, 1995; Priestley and Patton, 1997; Baker et al., 2004), In reality, significant shear energy is observed from explosions, but the full understanding of its generation remains relatively poor. A number of different sources have been proposed for the origin of shear energy in explosions, including the scattering and conversion of P-waves and surface waves (e.g., Walter et al., 1994; Myers et al., 1999), spall-induced Rg generation and conversion (e.g., Patton and Taylor, 1995; Patton et al., 2005), direct generation of S-waves in the source region (e.g., Fisk 2006; Baker et al., 2012), or some combination of these effects (e.g., Pitarka et al., 2015), but there is no broad community agreement on which mechanism or group of mechanisms is most important.

The Nevada National Security Site (NNSS; formerly the Nevada Test Site; NTS) in the Basin and Range Region of the western United States was the site of hundreds of nuclear explosions from 1951 until 1992 (U. S. Department of Energy, 2015). The focus of discrimination analysis of these historic events tended to be on the larger-magnitude explosions observed initially at teleseismic distances, then at regional distances. Additionally, underground nuclear testing was mostly carried out within a narrow range of scaled depths of burial (e.g., Denny and Johnson, 1991). To aid in the development of better explosion S-wave generation models, several recent series of chemical explosion experiments were carried out at the NNSS. The Source Physics Experiment Phase I (SPE) and Phase II (DAG – Dry Alluvium Geology), the Forensic Surface Events (FSE), the Large Surface Explosion Coupling Experiment (LSECE), and the Multi-Domain

Experiment (MDE) cover a range of emplacement conditions with varying geology, yield, depth of burial (DOB) and scaled depth of burial (SDOB).

Because a primary application of event discrimination would be for the purposes of detecting an underground nuclear test, it is important to understand the level of similarity between P/S ratios from chemical explosions and those from nuclear explosions. There are data that suggest that the two explosion types are indistinguishable (e.g., Denny and Johnson 1991; Stump et al., 1999), and that specifically P/S ratios from chemical explosions look the same as those from nuclear explosions (e.g., Walter et al., 1994; Walter et al., 1995). However, comparisons of chemical and nuclear events at local distances and from events that are small in magnitude are rare, and it is necessary to understand how these effects may play a role in discrimination. In the first part of this paper, we compare data from the SPE and DAG chemical explosions to historic nuclear data from the NNSS. We then utilize data from all of the new chemical experiment series to further explore how the different emplacement conditions of the chemical explosions affect P/S ratios at a range of local and regional distances.

Data

We utilize data from the SPE, DAG, FSE, LSECE, and MDE experiments. All events are single-fired chemical explosions located at the NNSS (Fig. 1). SPE consisted of six buried explosions detonated in a single emplacement hole in granite. Explosion depths ranged from 31 to 87 m and yields ranged from 89-5035 kg TNT equivalent, producing scaled depths of burial from 190 – 1550 m/kt^1/3 (Table 1). Note that for easier comparison to historic nuclear data, we calculate the scaled depths of burial using the chemical-to-nuclear, yield equivalency factor of 2 reported by Denny (1994) for the 1993 Non-Proliferation Experiment, so that for chemical explosions, the scaled depth is m/(2*kt)^(1/3). DAG was comprised of four buried explosions, also in a single emplacement hole, located in a dry alluvium geology, approximately 11.9 km from the SPE site. Depths for the DAG events ranged from 51-385 m with yields of approximately 900-51,000 kg and scaled depths of 188-3156 m/kt^1/3. The FSE experiments were located at the SPE site and consisted of four explosions situated at or slightly above the surface with yields of 87-1000 kg (Kim et al., 2018). LSECE consisted of two surface explosions co-located with the DAG site, each with a yield of approximately 992 kg. MDE consisted of six surface explosions, approximately 3.1 km southwest of the DAG/LSECE site, with yields of 44-4000 kg. Details for all explosions can be found in Table 1.

Two separate, temporary arrays of seismic stations were deployed for the SPE and DAG experiments. We utilize data from these arrays, excluding the geophone sensors which have a more limited frequency range and extremely short event-to-station distances. For SPE, the included instruments consist of three lines of stations extending from approximately 2-25 km to the south, southwest, and west of the SPE site (Townsend et al., 2017), and for DAG, lines extending roughly 40 km to the south, 55 km to the southwest, 25 km to the west and 10 km to the east of the DAG site. The FSE explosions were recorded by the SPE array and the LSECE and MDE explosions were recorded by the DAG array. In addition to these arrays, we examine data available at the Incorporated Research Institutions in Seismology (IRIS) from the many permanent networks operating in the region, including the University of Nevada, Reno's Southern Nevada (SN) and Northern Nevada (NN) networks, the University of Utah Regional Seismic Network (UU), the Southern California Seismic Network (CI), the US National Seismic Network (US), the International Miscellaneous Stations (IM), the Leo Brady Network (LB), and the Livermore Nevada Network (LNN). During the SPE experiment, some stations from the USArray's

Transportable Array (TA) were reoccupied and made a part of the SN network. Most of the 2011-2016 SPE network was dismantled and redeployed in a new configuration designed for the 2017-2019 DAG and 2020 LSECE events, so only a small number of stations exist that recorded usable data for all of the recent experiments due to the small sizes and the limited seismic coupling of the surface explosions. Most channels are broadband, but we also utilize a significant number of short period channels. However, instrument response removal should account for any instrument sensitivities at the lowest frequencies we consider.

Due to the weak coupling and/or stronger attenuation effects of the dry porous alluvium as compared to the saturated granite, the smallest DAG explosions had yields approximately 10 times larger than the smallest SPE explosion, but similar observable distance ranges. Pg and Lg phases were measured out to distances of roughly 100 km for SPE-1, SPE-4Prime, DAG-1, and DAG-3. Intermediate-yield events (SPE-2, SPE-3, and DAG-4) can generally be observed out to 200-300 km, and the largest explosions (SPE-5, SPE-6, and DAG-2) can be observed out to at least 400 km. Figure 1 shows the locations of the SPE/FSE, DAG/LSECE and MDE sites and the stations used in this study, color-coded by the experiments for which there was usable data.

For the purposes of comparison, we also include historic data from past underground nuclear tests and the 1993 Non-Proliferation Experiment (NPE). The NPE was an approximately 1-kt yield chemical explosion detonated in a tunnel 390 m underground and situated in a tuff geology at the NTS (Denny, 1994). Additionally, 303 historic NTS nuclear tests with a range of geologies, depths, and yields are used to look at Pg/Lg ratio behavior from nuclear explosions in an average sense. Data from the NPE and the nuclear tests are confined primarily to a small number of regional-distances stations, however, one nuclear test, Hazebrook, had usable recordings at local-distances, and is examined in more detail. Details for Hazebrook and the NPE are in Table 1.

P/S Ratio Methods

We focus on the crustal-traveling Pg and Lg phases than can be observed across the range of local to regional distances of interest. We note that at local distances, the packet of reflected and scattered S-waves is traditionally referred to as Sg, while Lg refers to a regional phase. However, Sg and Lg represent a continuous phase (e.g., Baker et al., 2012), and for purposes of continuity in our results, we do not make a distinction between Sg and Lg. The Pg phase has a window length determined by the group velocity of 5.0-6.0 km/s, and the Lg window has a group velocity of 3.0-3.6 km/s. Phases are handpicked by an analyst. At local distances, the analyst input can be especially important because slight deviations in actual velocity structure from the velocity model can produce significant offsets from the expect arrival time of an event relative to the length of the amplitude window. Instrument responses are removed, and waveforms are filtered by a series of narrow-band filters. Amplitudes are measured as the root-mean-square (RMS) value in the group velocity window. In order to be used, Pg amplitudes must have a signal-to-noise ratio (SNR) of 2 or greater compared to pre-event noise, where the noise is defined as the RMS amplitude of a 60-s window of data immediately before the first P arrival. Lg is required to have an SNR of at least 1.5 relative to pre-event noise, where the lower threshold is to allow for more measurements on the typically weaker explosion S-phases. To prevent inclusion of noise bursts and spurious signals in our data set, particularly at the high frequencies, we require phases to pass the SNR threshold for at least 3 consecutive frequency bands and discard any measurements at frequencies higher than the first band that fails to meet the SNR threshold. We use all three components for ratio calculation, except in some instances of single-component historic data or corrupted or unusable data from individual components.

We apply the MDAC (magnitude and distance correction) methodology (Walter and Taylor, 2001) to measured amplitudes before calculating ratios. At local distances this correction can be very small, but it becomes progressively more important as distance increases, and in order to compare ratios across a range of distances, we apply the correction to all data. We follow the same procedure described in Pyle and Walter (2019). Amplitudes, A, are assumed to be the frequency-domain product of a source term, S, a site term, P, a geometrical spreading term, G, and a path term, incorporating intrinsic and apparent attenuation, B:

$$A(\omega) = S(\omega)P(\omega)G(r)B(r,\omega)$$

where r is distance. The source term utilizes the Brune (1970) spectral shape for earthquakes. Geometrical spreading follows the formulation of Street et al. (1975). Path effects are modeled using the high-resolution 2D attenuation model for the Basin and Range region of Pyle et al. (2017). Site terms are typically determined empirically in conjunction with the attenuation model (e.g., Pasyanos et al., 2009; Pyle et al., 2017), and many stations in our dataset did not have an available term. On average, Pg and Lg site terms tend to cancel when the ratio is taken (Pyle and Walter, 2020), but as an additional test we compared ratio results using 29 stations from this study with site terms to ratios from the same data calculated without site terms (Fig. S1). While some differences in ratio values can be seen at individual stations, the average values and levels of scatter are nearly indistinguishable between the two sets of ratios, so we ignore site terms for the purposes of this paper.

Measured amplitudes are corrected for the source, path, and geometrical spreading effects. In log-space, the P/S ratio is calculated as log (corrected Pg) – log (corrected Lg) for individual components and the ratio from all three components are averaged to obtain the final ratio. After the MDAC correction, earthquake sources would be expected to have ratios that scatter around zero. Explosion sources, which should not be well-accounted for by the earthquake spectral shape, should theoretically have ratios greater than zero. In a discrimination setting, positive explosion ratios would ideally separate from near-zero earthquake ratios.

Chemical-Nuclear Comparison

In order to examine how the P/S ratio behavior from the buried chemical explosions might apply in a nuclear monitoring situation, we compare data from the SPE and DAG events to data from historic nuclear tests that took place at the NTS. To ensure relatively similar emplacement conditions for the comparison, we select a subset of nuclear tests that were located within 6 km of the SPE and DAG sites. Events were further restricted to a maximum depth of 450 m, to better match the shallow SPE chemical explosions and to ensure a detonation above the water table for better comparison to DAG. For the SPE comparison, seven nuclear events met these criteria; for DAG 54 events fit the criteria (Fig. 2a). A number of stations recorded the historic nuclear tests, however, due to the large size of nuclear test explosions and high historic gain settings on the instruments, much of the nuclear data is clipped and therefore unusable for P/S ratios. Four stations had data for both SPE or DAG events as well as a large number of non-clipped nuclear tests: DAC, ELK, KNB, and NV31 (formerly MNV). ELK, KNB, and NV31 are regional stations with distances from the SPE and DAG sites of approximately 410 km, 290 km, and 235 km, respectively, and DAC falls in the far-local regime with a distance of approximately 170 km (Fig. 2a).

Ratios from SPE and the nearby seven nuclear tests are in shown in Figure 2b, and the comparison of DAG and nearby nuclear tests are in Figure 2c. No SPE events were recorded well enough at KNB to obtain ratios, but ratios were obtained at DAC and NV31 for four of the SPE events (2,3,5,6) and at ELK for two events (5,6). Of the DAG events, only DAG-2 was recorded well-enough at all four stations to obtain ratios across a broad range of frequencies, although DAG-4 contributes ratios at the lowest frequencies at ELK, KNB, and NV31. The SPE ratios exhibit excellent consistency with nearby nuclear ratios across all frequency bands. DAG ratios fall well within the range of the nearby nuclear ratios, although the scatter among the nuclear ratios is considerable.

Due to the extensive clipping of the nuclear test data, few opportunities exist for comparison of P/S ratios from chemical and nuclear explosions at local distances. The Hazebrook event is the only nuclear test for which we found unclipped data with pickable Pg and Lg phases at stations that also recorded SPE or DAG data. Hazebrook was a M_L 2.2 event, which is comparably-sized to SPE-5 (M_L 2.1 – PDE) and DAG-2 (M_L 2.33 – NEIC). It consisted of three simultaneous explosions on February 2, 1987, at depths of 186 m, 226 m, and 262 m, located in alluvium geology, 4.59 km from the SPE site and 7.59 km from the DAG site (Springer et al., 2002). Stations WCT, MCA, GMN, and DAC all recorded Hazebrook and the SPE events, and DAC and GMN additionally recorded DAG events. Station distances from the Hazebrook event are 67 km for WCT, 108 km for GMN, 125 km for MCA, and 171 km for DAC.

Pg/Lg ratios from the Hazebrook, SPE, and DAG events are shown in Figure 3. Instrument response corrected and filtered (1-10 Hz) waveforms from Hazebrook and SPE-5 recorded at station GMN are shown in Figure 4. Both the waveforms and the ratios show remarkable similarity between SPE and the nuclear event. Ratios from the DAG events at DAC and GMN also compare favorably with the Hazebrook ratios, but it is notable that despite having a more similar geology to the DAG events (both are situated in alluvium), the Pg/Lg ratios for Hazebrook show generally better agreement with the more closely located SPE events.

P/S Ratio Observations

We calculate and MDAC correct the Pg/Lg ratios for all possible stations and each event in the SPE, DAG, FSE, LSECE, and MDE experiments. We plot the resulting ratios according to emplacement condition groups defined by the geology and buried or surface location for the explosions: hard rock buried explosions (HRB – contains SPE ratios), soft rock buried explosions (SRB – contains DAG ratios), hard rock surface explosions (HRS - contains FSE ratios) and soft rock surface explosions (SRS – contains LSECE and MDE ratios). The mean ratio values we obtain for each emplacement group are plotted in Figure 5. The ranges in the total number of ratios for each frequency-band/event-type combination that are available for the calculation of each average value are also shown. At frequencies higher than 4-6 Hz, ratios from all four experiments show strong similarity, despite variations in yield, contrasting geologies and ranges in depths of burial from the surface to significantly overburied (e.g., > 1000 m/kt^1/3). Also plotted are mean ratios from historic nuclear test data and the NPE chemical explosion. These ratios also compare favorably with the new experiments, despite the historic data being limited to mostly regional distances. Finally, mean ratios from the earthquake dataset of Pyle and Walter (2019) are also plotted to show their contrast from the explosion ratios. When averaged, all the explosions separate well from the earthquakes despite the large variation in their emplacements.

Ratios from each event-station combination, along with running averages for each emplacement group, are plotted as a function of event-to-station distance in Figure 6. The scatter in the individual ratios is very high, particularly at short distances, and decreases somewhat as distance increases. HRB and SRB ratios follow similar trends with distance, exhibiting, on average, positive values at the shortest distances, although significant outliers are present, then quickly dipping to near-zero by approximately 25-30 km, before rising again around 80-100 km. Beyond approximately 120-150 km, average ratios remain roughly constant. The distance range for which ratios are available is small for HRS and SRS due to the small size and weaker coupling of the surface events, however, they appear to follow similar trends as the HRB and SRB events, with initially high average ratios, significant outliers, and a downwards trend at approximately 30 km. In Figure 7 we plot the individual ratios as function of different factors in the emplacement conditions: yield, DOB, and SDOB. We observe no apparent trend in ratios with any of these factors, but again note an order of magnitude level of scatter in all instances.

The high level of scatter observed in the ratios is likely due at least in part to path effects. As described above, we apply a 2D attenuation model to account for these effects, however, there are certainly small-scale heterogeneities present which are likely to be smoothed out by the tomographic model but will impact local-distance amplitudes before their effects are significantly attenuated. To reduce the scatter due to these small-scale path effects, we compare ratios from pairs of explosions utilizing subsets of stations common to both explosions in the pair. SPE-5 and DAG-2 had the largest yields and the largest distance ranges for recording in the HRB and SRB emplacement groups. Figure 8a shows the stations that had usable ratios for both events and Figure 8b shows the mean Pg/Lg ratios calculated from this subset of stations as a function of frequency. The stations are common over the frequency range of 6-16 Hz; extending to higher or lower frequencies significantly reduces the number of stations that can be considered. The average ratios for both events exhibit strong similarity, as seen previously with the entire set of stations (Fig. 5).

To look for possible trends in ratios due to the contrasting geologies of the HRB and SRB emplacement groups, we plot the difference between the SPE-5 and DAG-2 ratios at each individual station in Figure 8c. No obvious trend in the differential ratios is present. However, when the differential ratios are plotted as a function of distance (Fig. 8d), we observe that above 8 Hz and beyond ~150 km, SPE-5 has a consistently higher ratio than DAG-2. This is consistent with observations by Walter et al. (1995), that historic nuclear explosions located at the NTS and situated in low-gas porosity/high-strength material, such as the water-saturated granite of SPE-5, exhibited higher ratios than those sited in high-gas porosity/low-strength material, such as the dry porous alluvium of DAG-2.

To take a further look at possible effects of DOB and SDOB on Pg/Lg ratios, we compare the shallowest and deepest events for the HRB events, for the SRB events, and for the deepest SRB event with a co-located surface SRS event at subsets of common stations. Mean ratios are plotted in Figure 9, along with the subsets of stations that are included in the average calculation. The deeper event (SPE-4Prime and DAG-1) has higher mean Pg/Lg ratios than the shallower event (SPE-6, DAG-1, and LSECE-2) in each case, however, the differences are very small and the overlap of the range of ratios is considerable. To further eliminate path effects other than those due to DOB, we again plot differential ratios at each station in Figure 10. The slightly higher Pg/Lg ratio for the deeper events, on average, remains in these plots, but the scatter of the differential ratios would suggest that there is not a clear trend associated with the DOB or SDOB.

Discussion and Conclusions

We have examined Pg/Lg ratios from a series of chemical explosion experiments at the NNSS to ascertain their similarity to ratios from nuclear test data and to assess the effects of differences in geology, yield, DOB, and SDOB at ranges of local and regional distances. We see strong similarity in Pg/Lg ratios from the chemical explosions to those from historic nuclear tests and the high-yield NPE chemical explosion. This result is consistent with a previous finding of likeness in ratios from the NPE to nuclear data by Walter et al. (1995), but our analysis extends this comparison to include local distances and smaller magnitude events. In particular, the small magnitude Hazebrook test shows excellent waveform similarity to SPE-5 and good ratio agreement with SPE and DAG events at local distance stations. The similarities of chemical and nuclear Pg/Lg ratios across yield and distance ranges suggests reasonable confidence that testing this discriminant with chemical explosions provides a good proxy for a nuclear monitoring situation.

As previously observed by Pyle and Walter (2019), we see large amounts of scatter in the ratios at short event-to-station distances, and a significant dip in the average ratio values starting at 25-30 km. Possibly, at these short distances, Rg contamination may be present in amplitude measurements resulting in reduced Pg/Lg ratios, but the scatter of low ratios persists at high frequencies and to distances of approximately 80-100 km. Rg is expected to attenuate quickly in the Basin and Range, and if it is present, Rg contamination is likely to be a less significant factor than structural effects in these low ratios. Recent work by Wang et al. (2021) demonstrated the effectiveness of path corrections at reducing scatter in Pg/Lg ratios at local distances using a Bayesian kriging method. We apply a 2D attenuation model to account for path effects, but it is clear that significant small-scale path effects remain and present a challenge for event discrimination at local distances.

We do not observe a strong trend in Pg/Lg ratios with DOB, although some previous studies have noted an increase in ratio with increasing DOB (e.g., Taylor et al., 1989; Myers et al., 1999). The Walter et al. (1995) study found that, at least for explosions located at the NTS, when the strength of material was accounted for, the changes in ratios with DOB were eliminated. Our data adds further support to this conclusion since the dry alluvium/weaker material situated DAG-2 event has a much deeper DOB (~300 m) than does the granite/stronger material emplaced SPE-5 event (~76 m), but exhibits lower ratios at common stations, pointing to material, not DOB, as the important factor. While this trend is not observed at distances shorter than approximately 150 km, it is possible that it is obscured by the scatter in the ratios. At short distances path differences from the SPE and DAG sites to individual stations can be significant, but as distance increases, the paths become very similar, allowing for the emergence of this trend at far-local and regional distances.

Although the differences are small, when comparing pairs of explosions with identical epicenters but differing DOBs, we observe, on average, that the shallower explosion source has slightly larger Pg/Lg ratios than deeper sources. This average disparity remains even when differential ratios at individual stations are considered to reduce path effects to variations only in DOB. However, the large amount of scatter in the individual differential ratios, and the near-zero average values, even for the large differences in DOB and SDOB for DAG-1 and DAG-4, is suggestive of weak to no dependence on these factors. Indeed, the scatter observed in differential ratios for the DAG-4 and DAG-1 comparison is nearly indistinguishable from that of the LSECE-2 and DAG-1 comparison. If DOB, SDOB, or related effects, such as spall, played a significant role in the Pg/Lg value, we would not expect to see ratios from the surface explosions to compare so similarly to those from buried shots.

In summary, the new experiments we consider cover a large range of emplacement conditions from the hard-rock granite geology to the contrasting dry alluvium geology, and the range in DOB and SDOB from detonations at the surface to those that are significantly overburied. In spite of these differences, we find that averaged Pg/Lg ratios remain quite robust as a discriminant for all these explosions. These empirical results indicate that discrimination between small explosions and earthquakes is possible if a sufficient number of stations to obtain a good average are available, no matter the explosion emplacement. Large amounts of scatter in the data suggest that individual path effects play a substantial role in the ratio, but on average, we detect little to no difference in ratio from yield, DOB, or SDOB. This observation holds when ratios of pairs of events are compared at individual stations to eliminate path effects other than depth differences. We do see differences due to geology, however, these differences do not become apparent until approximately 150 km, suggesting that individual path effects dominate at shorter distances. The weak dependence of local P/S ratios on these emplacement properties, and particularly the similarity of buried and surface explosion values is suggestive that rock damage does not play a major role in generation of these seismic waves. One caveat is that the explosions studied here are relatively small and shallowly buried and appear to have little evidence of tectonic release. For significantly deeper and/or larger explosions that may trigger tectonic stress release, rock damage may be a more important factor. This will be one of the subjects of investigation in the planned SPE Phase III experiment (e.g., Walter et al., 2012). These observations are currently limited to the NNSS and Basin and Range region, and more data is needed to understand if similar trends can be extended to other locations, but they provide an important set of data points and future work towards improving our explosion models will need to explain and reproduce the weak emplacement dependence observed here.

Data and Resources

Supplemental material for this article includes a figure showing the comparison of Pg/Lg ratios calculated with site terms to those calculated without site terms. Data used in this study were recorded by the Northern Nevada (NN) and Southern Nevada (SN Seismic Networks, operated by the University of Nevada, Reno, the USArray Transportable Array (TA) network, the Southern California Seismic Network (CI) operated by the Caltech Seismological Laboratory and the USGS, the Leo Brady Network (LB) operated by Sandia National Laboratories, the Livermore Nevada Network (LNN), the US National Seismic Network (US) operated by Albuquerque Seismological Laboratory and the USGS, and the University of Utah Regional Network (UU). Most data are available freely through the Incorporated Research Institutions for Seismology (IRIS) Data Management Center. Additional data from SPE and reports are also part of Assembled Datasets at IRIS (http://ds.iris.edu/SeismiQuery/assembled.phtml, last accessed July 2021 and search dataset named "Source Physics Experiment"). DAG and LSECE data and reports are expected to be released as an assembled dataset through IRIS in the near future. Figures were made using the Generic Mapping Tools Software [Wessel and Smith, 1998].

Acknowledgements

We would like to thank Rebecca Rodd and Terri Hauk for assistance with datasets and Doug Dodge and Doug Knapp for their dedicated programing efforts on the Regional Body-wave Amplitude Processing software. We thank Sean Ford for discussions about explosion seismic wave generation, and Ellen Syracuse for a thoughtful initial review of the manuscript. We also thank two anonymous reviewers for their constructive reviews. The Source Physics Experiment (SPE, DAG), the Large Surface Explosion Coupling Experiment (LSECE), and the Multi-Domain Experiment (MDE) would not have been possible without the support of many people from several organizations. The authors thank and acknowledge funding for LSECE from Defense Threat Reduction Agency (DTRA) and the Nuclear Arms Control (NACT) program. The authors also wish to express their gratitude to the National Nuclear Security Administration, Defense Nuclear Nonproliferation Research and Development (DNN R&D), and the SPE working group, a multi-institutional and interdisciplinary group of scientists and engineers. This work was performed under the auspices of the U.S. Department of Energy by Lawrence Livermore National Laboratory under Contract DE-AC52-07NA27344. This is LLNL contribution LLNL-JRNL-825777.

Declaration of Competing Interests

The authors acknowledge there are no conflicts of interest recorded.

References

Baker, G. E., J. Stevens, and H. Xu (2004). Lg group velocity: A depth discriminant revisited, *Bull. Seismol. Soc. Am*., **94**, 2, 722-739.

Baker, G. E., J. L. Stevens, and H. Xu (2012). Explosion shear-wave generation in high-velocity source media, *Bull. Seismol. Soc. Am*., **102**, 4, 1,301-1,319, doi:10.1785/0120110119.

Bottone, S., M. D. Fisk, and G. D. McCartor (2002). Regional seismic-event characterization using a Bayesian formulation of simple kriging, *Bull. Seismol. Soc. Am*., **92**, 6, 2,277–2,296.

Brune, J. (1970). Tectonic stress and the spectra from seismic shear wave earthquakes, *J. Geophys. Res*., **75**, 4,997-5,009.

Denny, M. D., and L. R. Johnson (1991). The explosion seismic source function: models and scaling laws reviewed, in *Explosion Source Phenomenology*, American Geophysical Monograph 65, 1-24.

Denny, M. D. (1994). Introduction: DOE Non-Proliferation Experiment in M. D. Denny and S. P. Stull (Editors), *Proc. of the Symposium on the Non-Proliferation Experiment (NPE): Results and Implications for Test Ban Treaties*, Rockville, Maryland, 19-21, April 1994.

Fisk, M. D. (2006). Source spectral modeling of regional P/S discriminants at nuclear test sites in China and the former Soviet Union, *Bull. Seismol. Soc. Am*., **96**, 6, 2,349-2,367, doi:10.1785/0120060023.

Goldstein, P. (1995). Slopes of P- to S-wave spectral ratios – A broadband regional seismic discriminant and a physical model, *Geophys. Res. Lett*., **22**, 23, 3,147-3,150.

Hartse, H., S. R. Taylor, W. S. Philips, and G. E. Randall (1997). A preliminary study of regional seismic discrimination in central Asia with an emphasis on western China, *Bull. Seismol. Soc. Am.*, **97**, 551-568.

He, X., L.-F. Zhao, X.-B. Xie and Z.-X. Yao, (2018). High precision relocation and event discrimination for the 3 September 2017 underground nuclear explosion and subsequent seismic events at North Korean test site, *Seismol. Res. Lett.*, **89**, 6, 2,042-2,048, doi: 10.1785/0220180164.

Kim, K., A. Rodgers, and D. Seastrand (2018). Local infrasound variability related to in situ atmospheric observation, *Geophys. Res. Lett.*, **45**, 2,954-2,962, doi:10.1002/2018GL077124.

Kim, W.-Y., D. W. Simpson, and P. G. Richards (1993). Discrimination of earthquakes and explosions in the eastern United States using regional high frequency data, *Geophys. Res. Lett.*, **20**, 1,507-1,510, doi: 10.1029/93GL01267.

Kim, W.-Y., P. G. Richards, D. Schaff, E. Jo and Y. Ryoo (2018). Identification of seismic events on and near the North Korean test site after the underground nuclear test explosion of 3 September 2017, *Seismol. Res. Lett.*, **89**, 6, 2,120-2,130, doi: 10.1785/0220180133.

Ma, X., L. F. Zhao, X. B. Xie, X. He, and Z. X. Yao (2020). Regional seismic characteristics of chemical explosions on the Eastern margin of the Junggar Basin, Northwest China, and of historical Semipalatinsk nuclear tests, *Bull. Seismol. Soc. Am.,* **111**, 606-620, doi: 10.1785/0120200151.

Myers, S. C., W. R. Walter, K. Mayeda, and L. Glenn (1999). Observations in support of Rg scattering as a source for explosion S waves: regional and local recordings of the 1997 Kazakhstan depth of burial experiment, *Bull. Seismol. Soc. Am.*, **89**, 2, 544-549.

O'Rourke, C. T., G. E. Baker, and A. F. Sheehan (2016). Using P/S amplitude ratios for seismic discrimination at local distances, *Bull. Seismol. Soc. Am.*, **105**, 5, 2,320-2331, doi: 10.1785/0120160035.

Pasyanos, M. E., and W. R. Walter (2009). Improvements to regional explosion identification using attenuation models of the lithosphere, *Geophys. Res. Lett.*, **36**, L14304, doi:10.1029/2009GL038505.

Pasyanos, M. E., E. M. Matzel, W. R. Walter, and A. J. Rodgers (2009). Broad-band Lg attenuation modelling in the Middle East, *Geophys. J. Int.*, *177*, 1,166-1,176, doi:10.1111/h.1365-246X.2009.04128.x.

Pasyanos, M. E., S. R. Ford, and W. R. Walter (2014). Testing event discrimination over broad regions using the historical Borovoye Observatory explosion dataset, *Pure Appl. Geophys.*, **171**, 523-535, doi:10.1007/s00024-012-0591-4.

Patton, H. J., and S. R. Taylor (1995). Analysis of Lg spectral ratios from NTS explosions: implications for the source mechanisms of spall and the generation of Lg waves, *Bull. Seismol. Soc. Am.*, **85**, 1, 220-236.

Patton, H. J., J. L. Bonner, and I. N. Gupta (2005). Rg excitation by underground explosions: insights from source modelling the 1997 Kazakhstan depth-of-burial experiment, *Geophys. J. Int.*, **163**, 1,006-1,024, doi:10.1111/j.1365-246X.2005.02752.x.

Pitarka, A., R. J. Mellors, W. R. Walter, S. Ezzedine, O. Vorobiev, T. Antoun, J. L. Wagoner, E. M. Matzel, S. R. Ford, A. J. Rodgers, L. Glenn, and M. Pasyanos (2015). Analysis of ground motion from an underground chemical explosion, *Bull. Seismol. Soc. Am.*, **105**, 5, 2,390-2,410, doi:10.1785/0120150066.

Priestley, K. F., and H. J. Patton (1997). Calibration of m_b(Pn), m_b(Lg) scales and transportability of the M_0:m_b discriminant to new tectonic regions, *Bull. Seismol. Soc. Am.*, **87**, 5, 1,083-1,099.

Pyle, M. L., and W. R. Walter (2019). Investigating the effectiveness of P/S amplitude ratios for local distance event discrimination, *Bull. Seismol. Soc. Am.*, **109**, 3, 1,071-1,081, doi:10.1785/0120180256.

Pyle, M. L., and W. R. Walter (2020). Understanding scatter in local-distance event amplitude predictions and implications for event discrimination, S045-0015 presented at 2020 Fall Meeting, AGU, San Francisco, CA, 1-17 Dec.

Pyle, M. L., W. R. Walter, and M. E. Pasyanos (2017). High-Resolution 2D Lg and Pg attenuation models in the Basin and Range region with implications for frequency-dependent Q, *Bull. Seismol. Soc. Am.*, **107**, 6, 2,846-2,858, doi:10.1785/0120170172.

Rodgers, A. J., W. R. Walter, C. A. Schultz, S. C. Myers, and T. Lay (1999). A Comparison of methodologies for representing path effects on regional P/S discriminants, *Bull. Seismol. Soc. Am.*, **82**, 2, 394-408.

Rodgers, A. J., and W. R. Walter (2002). Seismic discrimination of the May 11, 1998 Indian nuclear test with short-period regional data from station NIL (Nilore, Pakistan), *Pure Appl. Geophys.,* **159**, 679-800.

Springer, D. L., G. A. Pawloski, J. L. Ricca, R. F. Rohrer, and D. K. Smith (2002). Seismic source summary for all U. S. below-surface nuclear explosions, *Bull. Seismol. Soc. Am.*, **92**, 5, 1,806-1,840.

Street, R. L., R. B. Herrmann, and O. W. Nuttli (1975). Spectral characteristics of the Lg wave generated by central United States earthquakes, *Geophys. J. R. Astr. Soc.*, **41**, 51-63.

Stump, B. W., D. C. Pearson, and R. E. Reinke (1999). Source comparisons between nuclear and chemical explosions detonated at Rainier Mesa, Nevada Test Site, *Bull. Seismol. Soc. Am.*, **89**, 2 409-422.

Taylor, S. (1996). Analysis of high-frequency Pg/Lg rations from NTS explsions and western U.S. earthquakes, *Bull. Seismol. Soc. Am.*, **86**, 1,042-1,053.

Taylor, S. R., M. D. Denny, E. S. Vergino, and R. E. Glaser (1989). Regional discrimination between NTS explosions and western U. S. earthquakes, *Bull. Seismol. Soc. Am.*, **79**, 5, 1,142-1,176.

Taylor, S. R., and H. E. Hartse (1998). A Procedure for estimation of source and propagation amplitude corrections for regional seismic discriminants, *J. Geophys. Res.*, **103**, B2, 2,781-2,789.

Townsend, M. and C. Obi (2017). Data release report for Source Physics Experiment 4Prime (SPE-4Prime) Nevada National Security Site Revision 1, National Security Technologies, LLC, Technical Report DOE/NV/25946—3311-REV-1, 70pp. Las Vegas, NV.

U.S. Department of Energy (2015). United States Nuclear Tests July 1945 through September 1992, U.S. Department of Energy, National Nuclear Security Administration Field Office Publication, DOE/NV—2090REV16 available at https://www.nnss.gov/docs/docs_LibraryPublications/DOE_NV-209_Rev16.pdf (last accessed 07/23/2021).

Walter, W. R., K. Mayeda, and H. J. Patton (1994). Regional seismic observations of the non-proliferation experiment at the Livermore NTS network in M. D. Denny and S. P. Stull (Editors), *Proc. of the Symposium on the Non-Proliferation Experiment (NPE): Results and Implications for Test Ban Treaties*, Rockville, Maryland, 19-21, April 1994.

Walter, W. R., K. Mayeda, and H. J. Patton (1995). Phase and spectral ratio discrimination between NTS earthquakes and explosions. Part I: Empirical observations, *Bull. Seismol. Soc. Am.*, **85**, 1,050-1,067.

Walter, W. R. and S. R. Taylor (2001). A revised Magnitude and Distance Amplitude Correction (MDAC2) procedure for regional seismic discriminants: theory and testing at NTS, Lawrence Livermore National Laboratory technical report, UCRL-ID-146882, available at http://www.llnl.gov/tid/lof/documents/pdf/240563.pdf (last accessed 09/12/2018).

Walter, W. R., M. L. Pyle, S. R. Ford, S. C. Myers, K. D. Smith, C. Snelson, and V. Chipman, (2012). Rock Valley direct earthquake-explosion comparison experiment (RV-DC): Initial feasibility study, Lawrence Livermore National Laboratory Technical Report, LLNL-TR-585672, 23 pp. https://doi.org/10.2172/1053650.

Walter, W. R., D. A. Dodge, G. Ichinose, S. C Myers, M. E. Pasyanos and S. R. Ford, (2018). Body-wave methods of distinguishing between explosions, collapses, and earthquakes: application to recent events in North Korea, *Seismol. Res. Lett.*, **89**, 6, 2,131-2,138, doi: 10.1785/0220180128.

Wang, R., B. Schmandt, and E. Kiser (2020). Seismic discrimination of controlled explosions and earthquakes near Mount St. Helens using P/S ratios, *J. Geophys. Res.: Solid Earth*, **125**, e2020JB020338, doi:10.1029/2020JB020338.

Wang, T., Y. Bian, Q. Yang, and M. Ren (2021). Correction of P/S amplitude ratios for low-magnitude seismic events based on Bayesian kriging method, *Bull. Seismol. Soc. Am.*, doi:10.1785/0120200293.

Wessel, P., and W. H. F. Smith (1998). New, improved version of the Generic Mapping Tools released, *Eos Trans. AGU*, **79**, 579.

Authors

Moira L. Pyle
Lawrence Livermore National Laboratory
7000 East Ave.
Livermore, CA 94550
pyle4@llnl.gov
925-423-4988

William R. Walter
Lawrence Livermore National Laboratory
7000 East Ave.
Livermore, CA 94550
walter5@llnl.gov
925-423-8777

Table 1. List of Chemical Explosions and the Hazebrook Nuclear Test

Event Name	Date	Hour (UTC)	Min	Sec	Latitude	Longitude	Yield (kg, TNT equivalent)	Depth (m)	SDOB† ($m/kt^{(1/3)}$)	Emplacement Group
SPE-1	05/03/11	22	0	0.011	37.2212	–116.0609	90	55.1	976	HRB
SPE-2	10/25/11	19	0	0.012	37.2212	–116.0609	997	45.7	363	HRB
SPE-3	07/24/12	18	0	0.448	37.2212	–116.0609	905	47.2	387	HRB
SPE-4Prime	05/21/15	18	36	0.000	37.2212	–116.0609	89	87.2	1550	HRB
SPE-5	04/26/16	20	49	0.000	37.2212	–116.0609	5035	76.5	354	HRB
SPE-6	10/12/16	18	36	0.000	37.2212	–116.0609	2245	31.4	190	HRB
DAG-1	07/20/18	16	51	52.678	37.1146	-116.0693	908	385.0	3156	SRB
DAG-2	12/19/18	18	45	56.921	37.1146	-116.0693	50997	299.8	642	SRB
DAG-3	04/27/19	15	49	1.842	37.1146	-116.0693	908	150.0	1229	SRB
DAG-4	06/22/19	21	6	19.876	37.1146	-116.0693	10357	51.6	188	SRB
FSE-1	11/29/16	20	10	0.000	37.2213	-116.0609	87	0	0	HRS
FSE-2	11/30/16	20	6	0.000	37.2213	-116.0609	87	-2	0	HRS
FSE-3	12/01/16	20	36	0.000	37.2213	-116.0609	100	-2	0	HRS
FSE-4	12/05/16	20	36	0.000	37.2213	-116.0609	1000	0	0	HRS
LSECE-1	10/27/20	13	37	10.638	37.1149	-116.0691	992.05	0	0	SRS
LSECE-2	10/29/20	22	35	34.313	37.1149	-116.0691	991.5	0	0	SRS
MDE-1	09/29/20	18	59	59.923	37.0999	-116.0986	44	0	0	SRS
MDE-2	10/01/20	20	59	59.922	37.0999	-116.0986	44	0	0	SRS
MDE-3	10/06/20	18	59	59.923	37.0999	-116.0986	88	0	0	SRS
MDE 4	10/07/20	20	19	59.918	37.0999	-116.0986	88	0	0	SRS
MDE 5	11/04/20	20	39	59.916	37.0999	-116.0986	88	0	0	SRS
MDE-6	11/07/20	17	39	59.928	37.0999	-116.0986	4000	0	0	SRS
NPE	09/22/93	07	00	01.080	37.2019	-116.2099	1000000	390	390	-
Hazebrook	02/03/87	15	20	00.08	37.181	-116.049	<20000000*	186-262*	-	-

* Yield and depth ranges of the nuclear test Hazebrook from U. S. Department of Energy, 2015

†Scaled depths of burial are calculated using the chemical-to-nuclear yield equivalency factor of 2.0 reported by Denny (1994)

List of Figure Captions

Figure 1. Map of stations used in the study. Black star shows the location of the SPE and FSE explosions, white star shows the location of the DAG and LSECE explosions, and gray star shows the location of the MDE explosions. Triangles show station locations and are color-coded by the experiments for which they have Pg/Lg ratios. Thick white outline shows the boundaries of the NNSS.

Figure 2. Comparison of Pg/Lg ratios from SPE and DAG events to historic nuclear data. (a) Map of stations (green triangles) that are used for the historic nuclear data. SPE and DAG locations are shown by the orange and yellow diamonds, respectively. Thick white outline shows the boundaries of the NNSS. In the map inset, orange stars show locations of nuclear events that are compared to the SPE events, and yellow stars shows nuclear events that are compared to the DAG events. (b) Comparison of Pg/Lg ratios of SPE events (orange diamonds) to nuclear tests (red stars). (c) Comparison of Pg/Lg ratios of DAG events (yellow diamonds) to nuclear tests (red stars).

Figure 3. Comparison of Pg/Lg ratios from the Hazebrook nuclear test (red stars) to SPE (orange diamonds) and DAG (yellow diamonds) events at local-distance stations (a) DAC, (b) GMN, (c) MCA, and (d) WCT.

Figure 4. Comparison of velocity waveforms from the Hazebrook nuclear test (black) and SPE-5 (red) at station GMN, approximately 107 km away. (a) Entire waveform and (b) zoomed in view

of P-waves. Waveforms have been corrected for instrument response and filtered between 1 and 10 Hz.

Figure 5. Mean Pg/Lg ratios from hard-rock buried explosions (HRB - orange diamonds), soft-rock buried explosions (SRB - yellow diamonds), hard-rock surface explosions (HRS - dark green diamonds), soft-rock surface explosions (SRS - light green diamonds), NPE (purple diamonds), historic nuclear tests (red stars) and earthquakes from the Pyle and Walter (2019) study (blue circles). Means are calculated using all possible ratios for each emplacement group/experiment. Error bars represent one standard deviation. Numbers beneath each symbol in the legend indicate the range in numbers of ratios across the different frequency bands that are available for the mean calculation for each event type.

Figure 6. Pg/Lg ratios from individual stations and events as a function of distance at (a) 2-4 Hz, (b) 6-8 Hz, (c) 12-16 Hz. Top row shows the scatter of ratios, bottom row shows a running average of the ratios for each experiment. Scales are the same across all plots. Symbols and colors are the same as for Figure 5.

Figure 7. Pg/Lg ratios plotted as functions of yield, depth of burial, and scaled depth of burial at several frequency bands. Symbols and colors are the same as for Figure 5.

Figure 8. Comparison of Pg/Lg ratios from SPE-5 and DAG-2 at a subset of stations common to both events. (a) Map of stations included in the subset. (b) Average Pg/Lg ratios for each event calculated using the subset of stations. Symbols and colors are the same as for Figure 5, and error

bars represent one standard deviation. (c) Differential Pg/Lg ratios from SPE-5 and DAG-2 at individual stations shown as black diamonds. (d) Differential ratios as a function of distance at a few frequency bands.

Figure 9. Comparison of pairs of events at common subsets of stations. (a) Mean Pg/Lg ratios from SPE-4Prime and SPE-6 and map of stations that are used in the mean calculation. (b) Mean ratios and stations from DAG-1 and DAG-4. (c) Mean ratios and stations from LSECE-2 and DAG-1. In each case the yellow diamonds represent the shallower of the two events and the purple diamonds represent the deeper event. Error bars represent one standard deviation. Gray-shaded areas cover frequencies for which all stations are common for both events.

Figure 10. Differential Pg/Lg ratios for DAG-4 and DAG-1 (yellow diamonds) and LSECE-2 and DAG-1 (green diamonds).

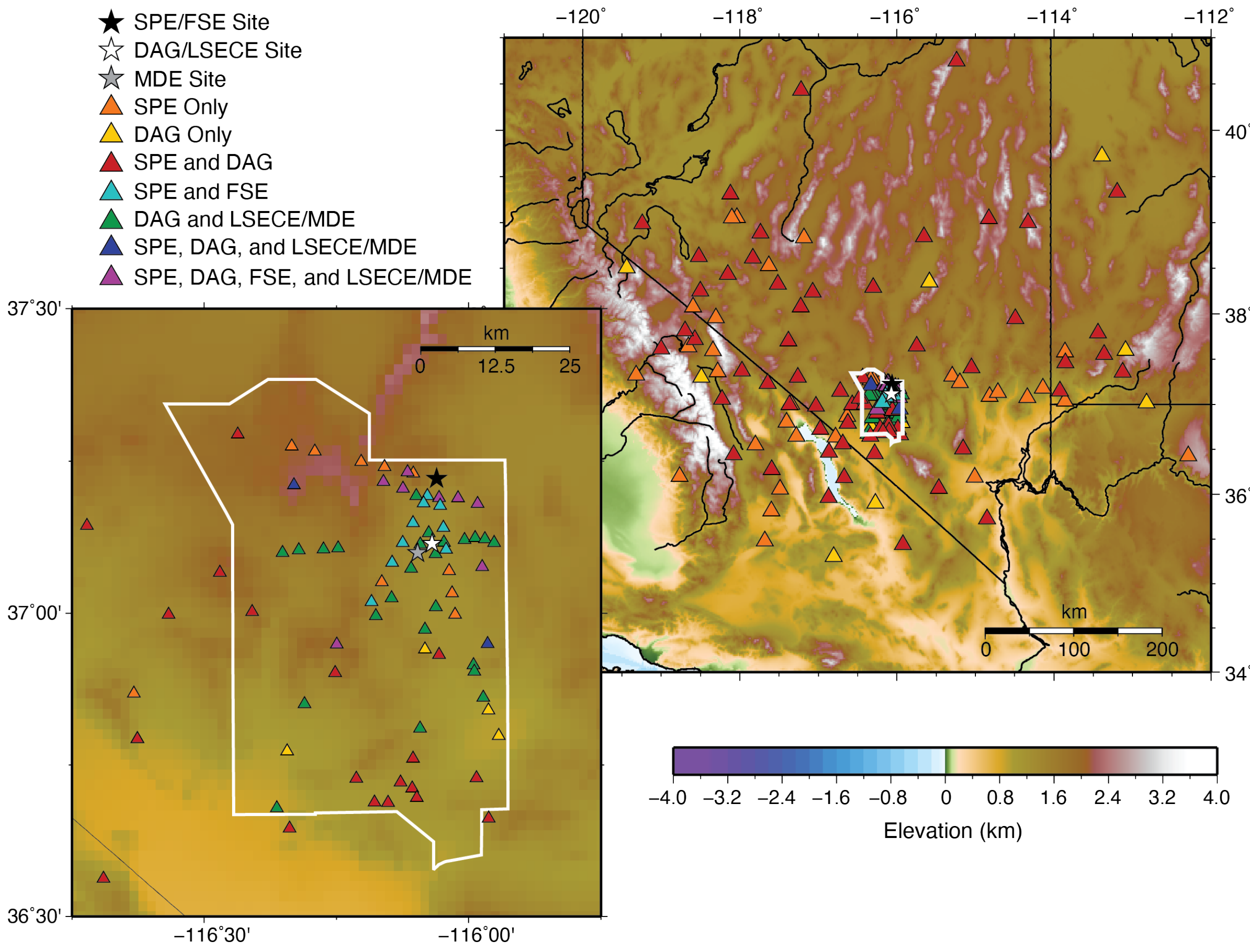

Figure 1. Map of stations used in the study. Black star shows the location of the SPE and FSE explosions, white star shows the location of the DAG and LSECE explosions, and gray star shows the location of the MDE explosions. Triangles show station locations and are color-coded by the experiments for which they have Pg/Lg ratios. Thick white outline shows the boundaries of the NNSS.

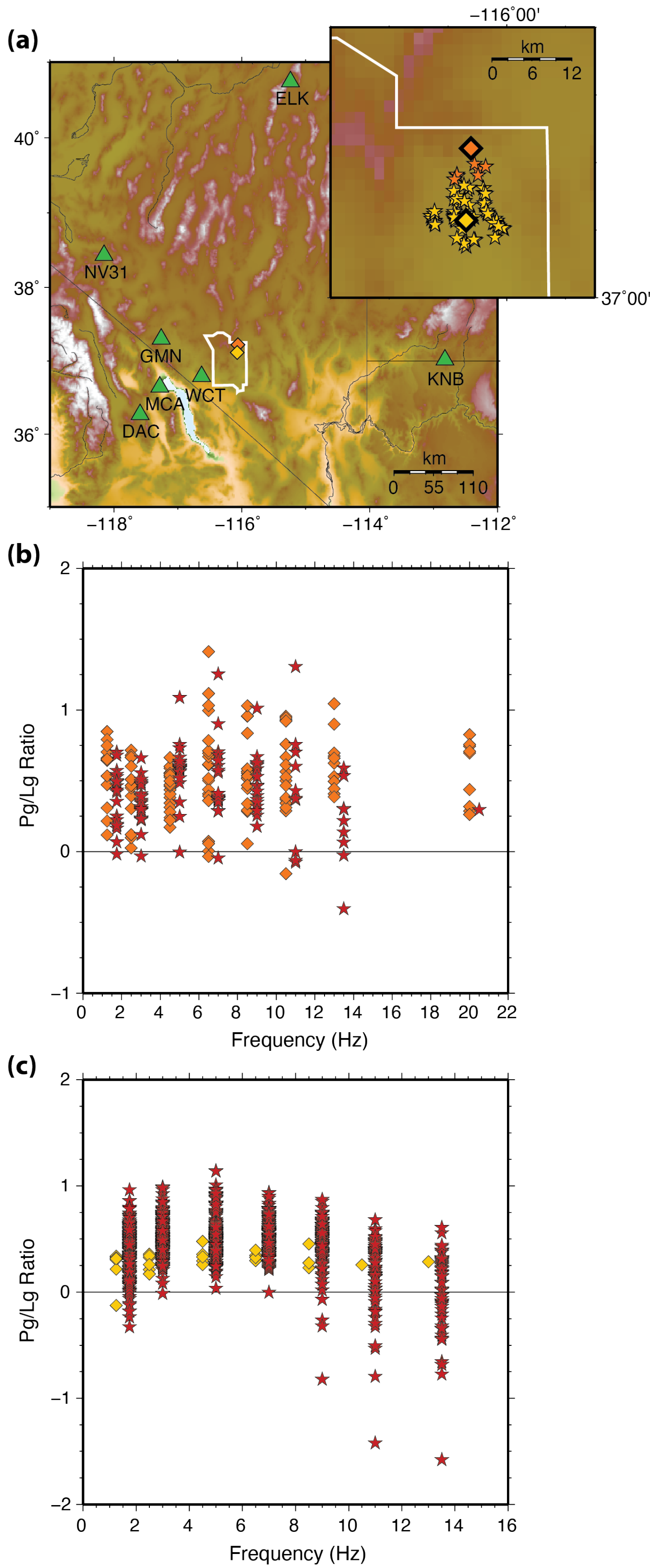
(a)
–116˚00'
km
0 6 12
37˚00'
ELK
40˚
NV31
38˚
GMN
WCT
MCA
DAC
KNB
36˚
km
0 55 110
–118˚
–116˚
–114˚
–112˚
(b)
Pg/Lg Ratio
Frequency (Hz)
(c)
Pg/Lg Ratio
Frequency (Hz)

645

Figure 2. Comparison of Pg/Lg ratios from SPE and DAG events to historic nuclear data. (a) Map of stations (green triangles) that are used for the historic nuclear data. SPE and DAG locations are shown by the orange and yellow diamonds, respectively. Thick white outline shows the boundaries of the NNSS. In the map inset, orange stars show locations of nuclear events that are compared to the SPE events, and yellow stars shows nuclear events that are compared to the DAG events. (b) Comparison of Pg/Lg ratios of SPE events (orange diamonds) to nuclear tests (red stars). (c) Comparison of Pg/Lg ratios of DAG events (yellow diamonds) to nuclear tests (red stars).

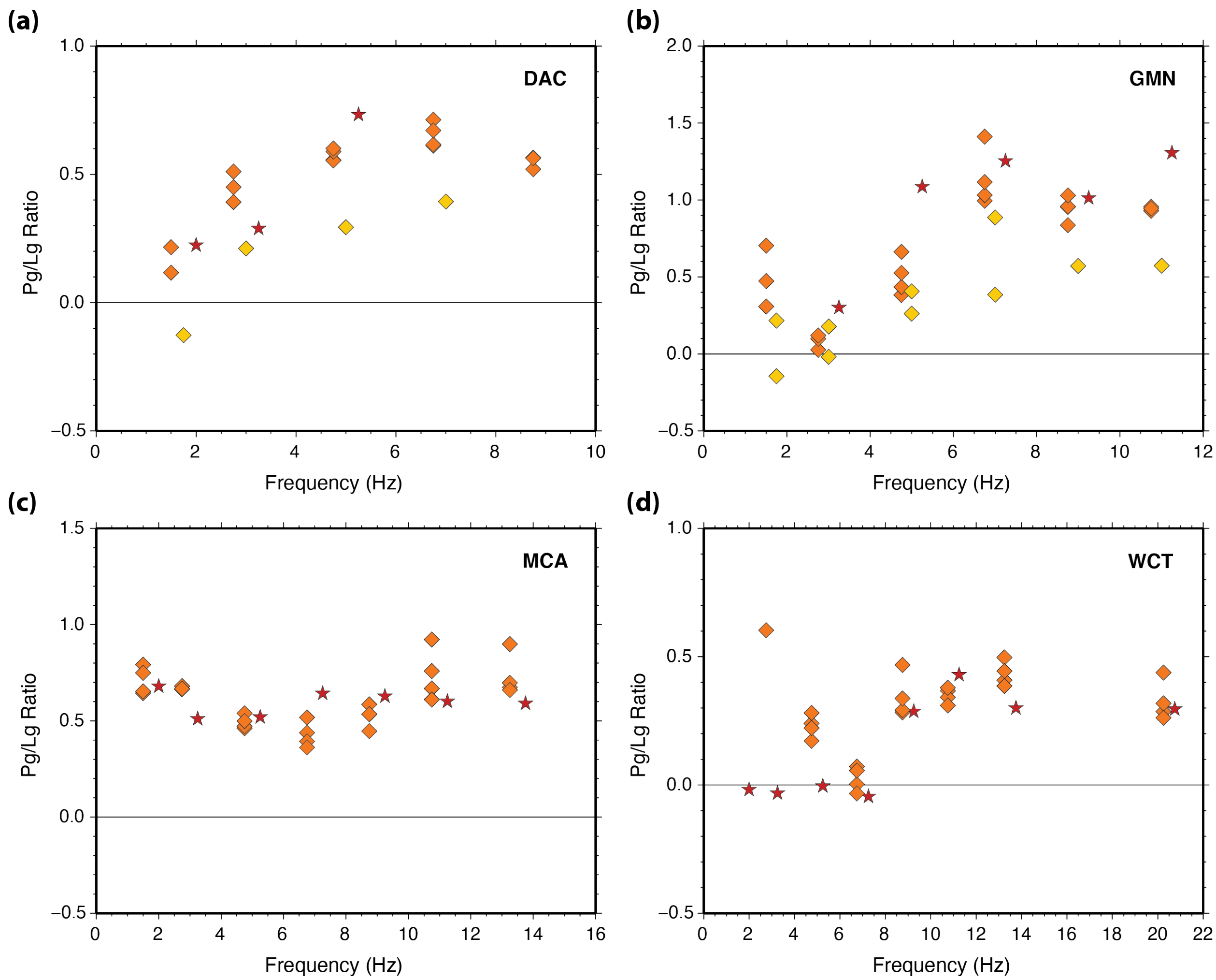

Figure 3. Comparison of Pg/Lg ratios from the Hazebrook nuclear test (red stars) to SPE (orange diamonds) and DAG (yellow diamonds) events at local-distance stations (a) DAC, (b) GMN, (c) MCA, and (d) WCT.

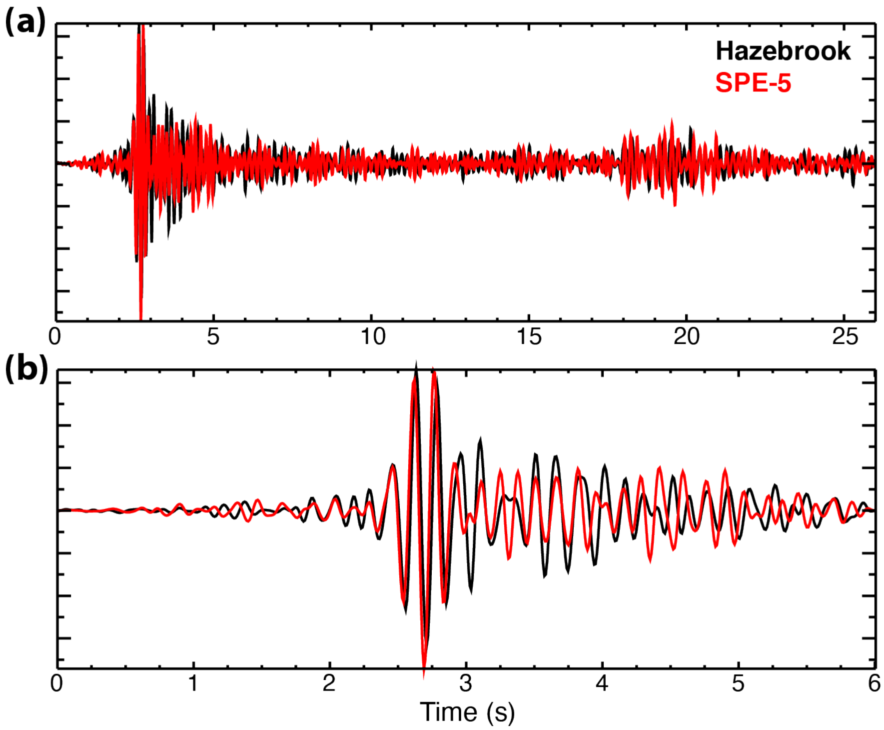

Figure 4. Comparison of velocity waveforms from the Hazebrook nuclear test (black) and SPE-5 (red) at station GMN, approximately 107 km away. (a) Entire waveform and (b) zoomed in view of P-waves. Waveforms have been corrected for instrument response and filtered between 1 and 10 Hz.

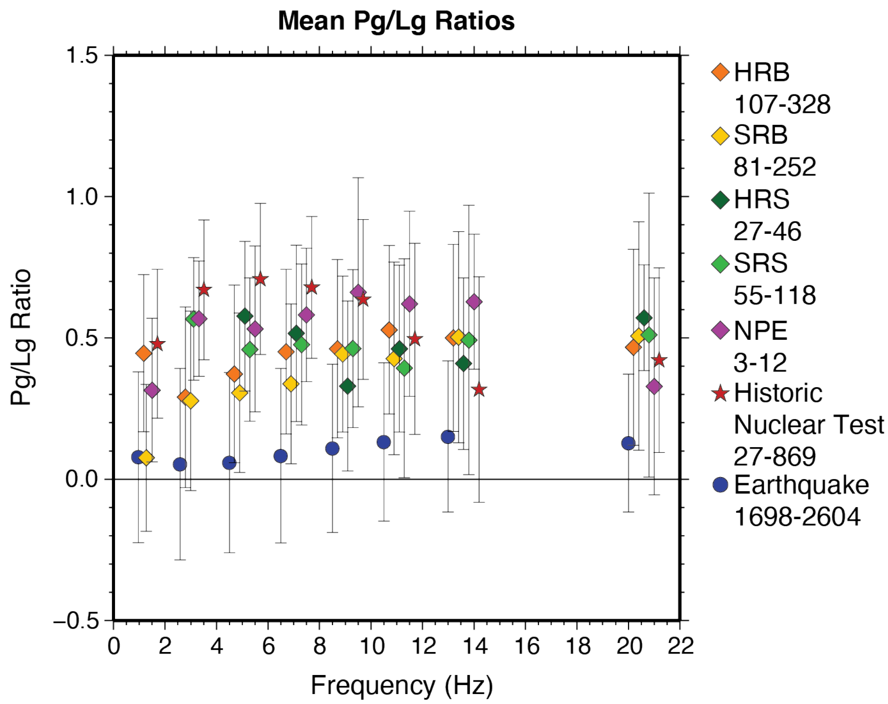

Figure 5. Mean Pg/Lg ratios from hard-rock buried explosions (HRB - orange diamonds), soft-rock buried explosions (SRB - yellow diamonds), hard-rock surface explosions (HRS - dark green diamonds), soft-rock surface explosions (SRS - light green diamonds), NPE (purple diamonds), historic nuclear tests (red stars) and earthquakes from the Pyle and Walter (2019) study (blue circles). Means are calculated using all possible ratios for each emplacement group/experiment. Error bars represent one standard deviation. Numbers beneath each symbol in the legend indicate the range in numbers of ratios across the different frequency bands that are available for the mean calculation for each event type.

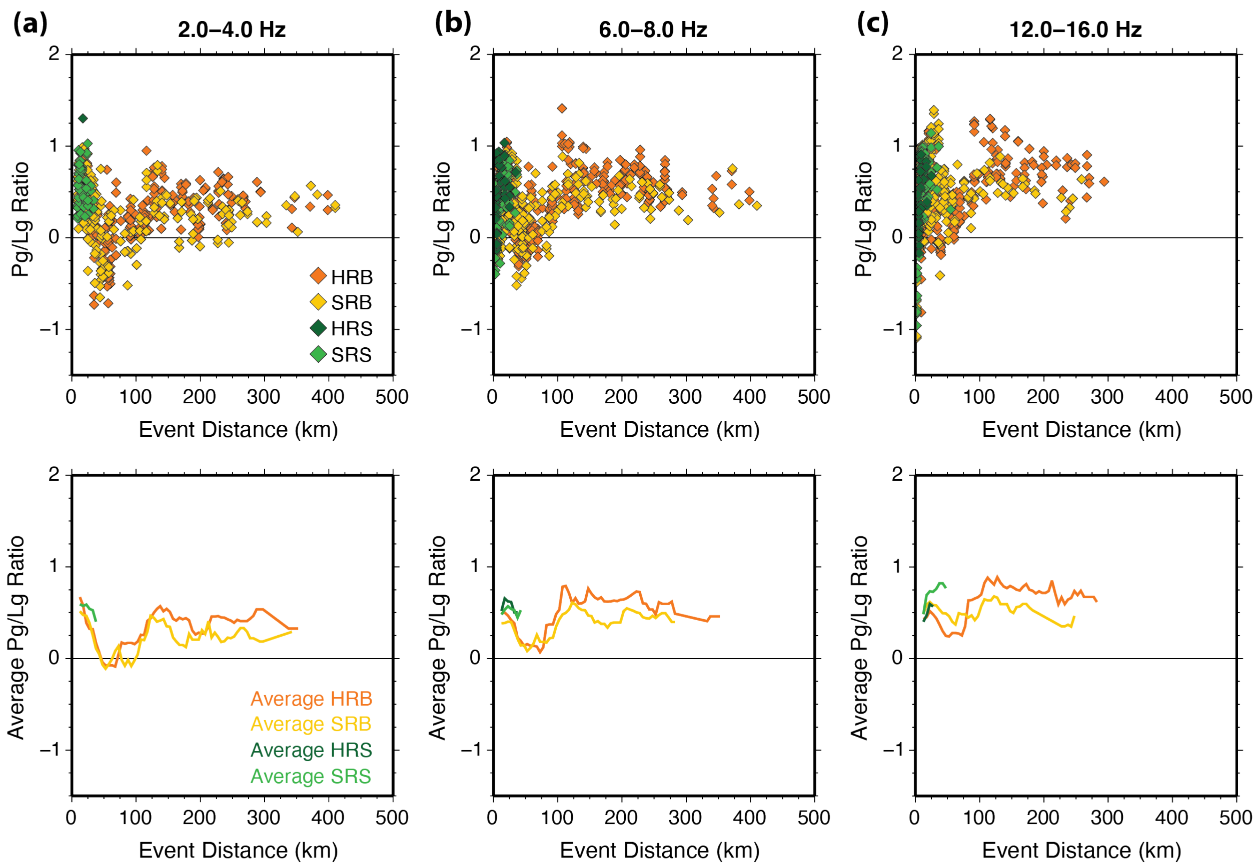

Figure 6. Pg/Lg ratios from individual stations and events as a function of distance at (a) 2-4 Hz, (b) 6-8 Hz, (c) 12-16 Hz. Top row shows the scatter of ratios, bottom row shows a running average of the ratios for each experiment. Scales are the same across all plots. Symbols and colors are the same as for Figure 5.

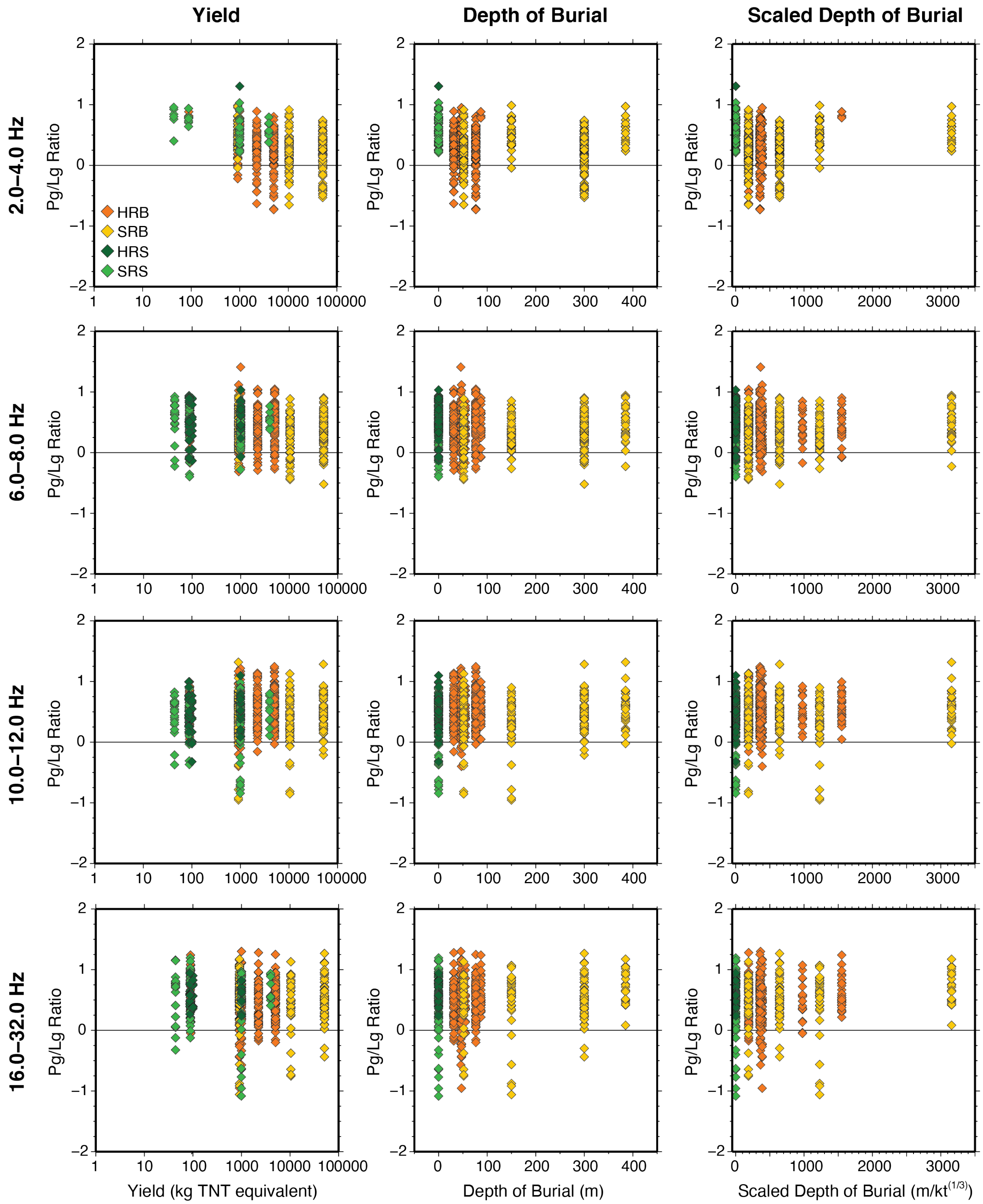

Figure 7. Pg/Lg ratios plotted as functions of yield, depth of burial, and scaled depth of burial at several frequency bands. Symbols and colors are the same as for Figure 5.

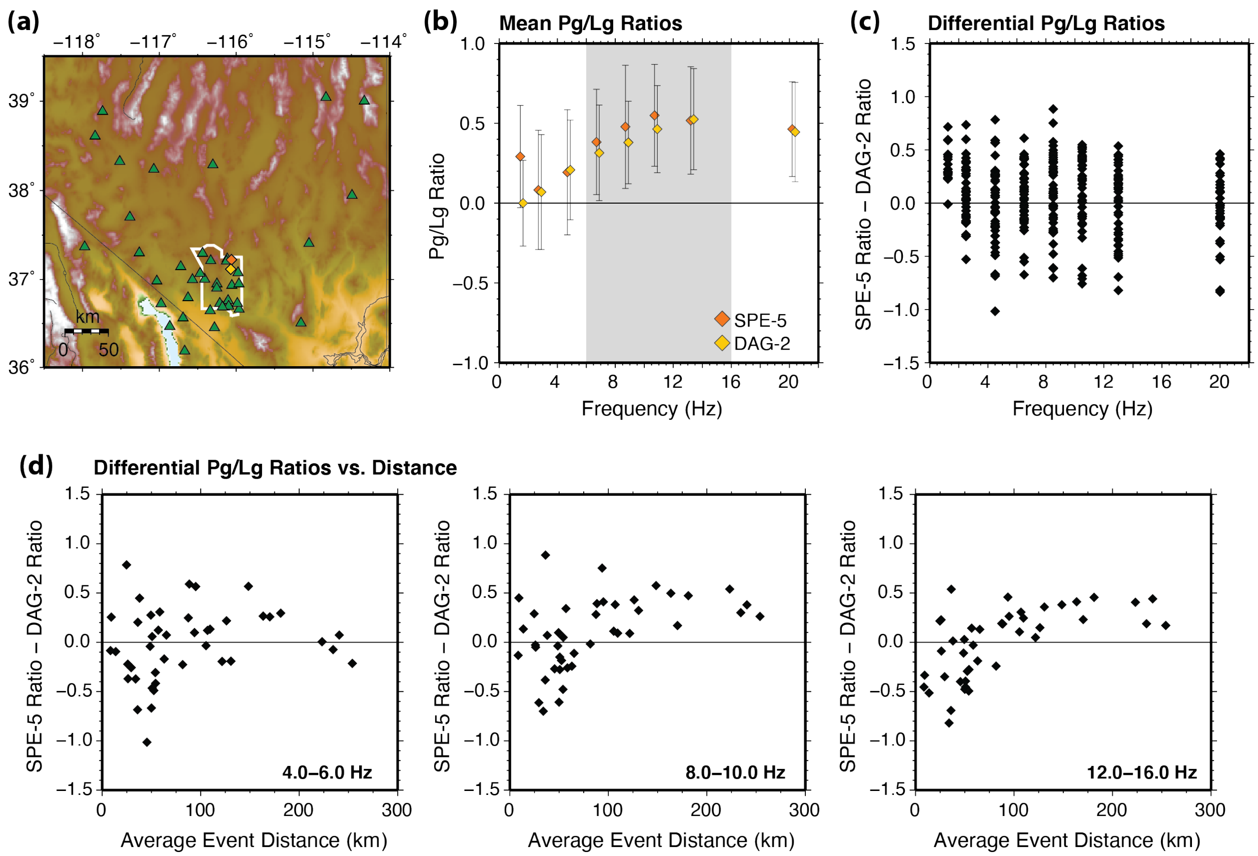

Figure 8. Comparison of Pg/Lg ratios from SPE-5 and DAG-2 at a subset of stations common to both events. (a) Map of stations included in the subset. (b) Average Pg/Lg ratios for each event calculated using the subset of stations. Symbols and colors are the same as for Figure 5, and error bars represent one standard deviation. (c) Differential Pg/Lg ratios from SPE-5 and DAG-2 at individual stations shown as black diamonds. (d) Differential ratios as a function of distance at a few frequency bands.

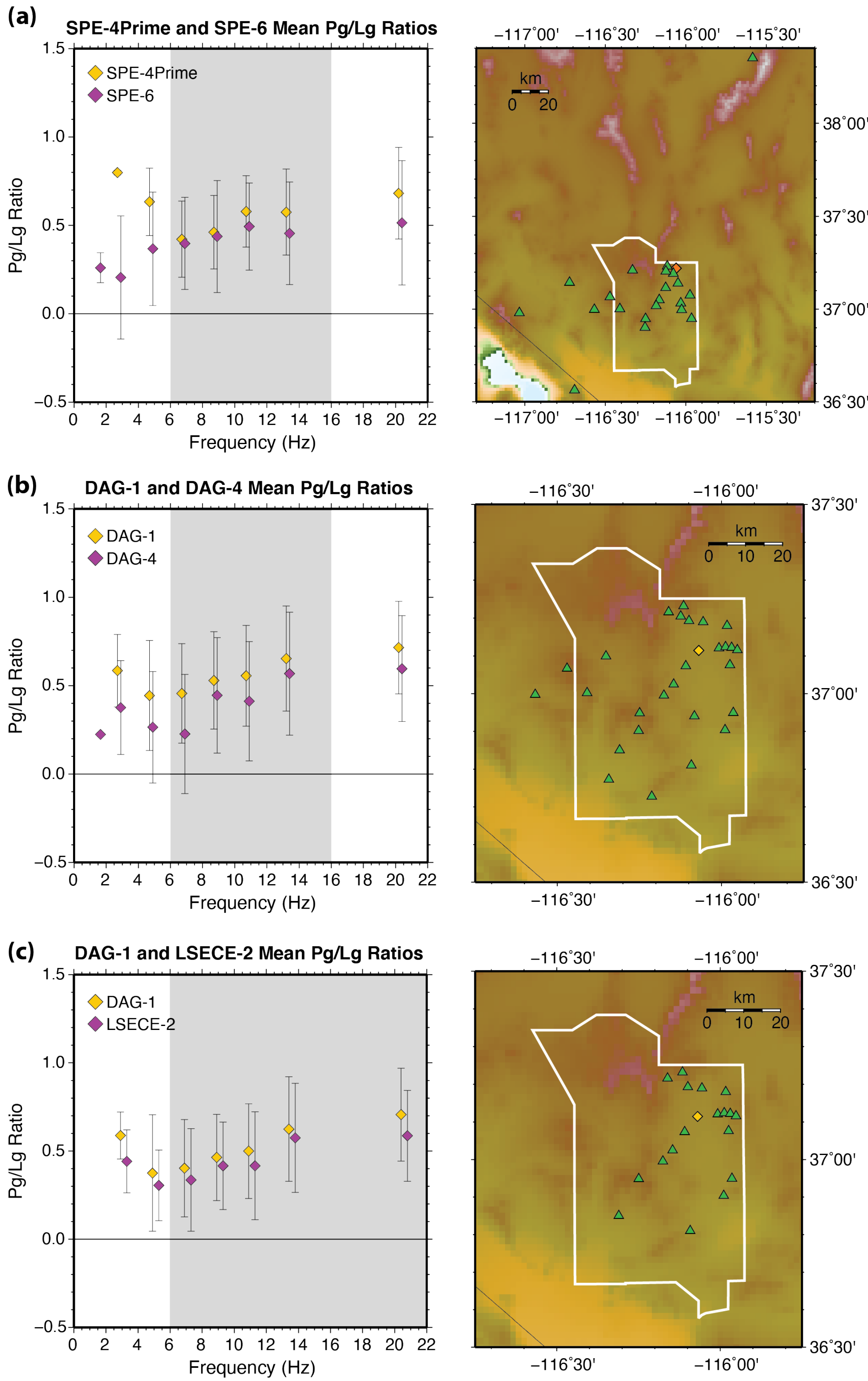

(a)
SPE-4Prime and SPE-6 Mean Pg/Lg Ratios
SPE-4Prime
SPE-6
Pg/Lg Ratio
Frequency (Hz)
−117˚00' −116˚30' −116˚00' −115˚30'
38˚00'
37˚30'
37˚00'
36˚30'
km
0 20
(b)
DAG-1 and DAG-4 Mean Pg/Lg Ratios
DAG-1
DAG-4
Pg/Lg Ratio
Frequency (Hz)
−116˚30' −116˚00'
37˚30'
37˚00'
36˚30'
km
0 10 20
(c)
DAG-1 and LSECE-2 Mean Pg/Lg Ratios
DAG-1
LSECE-2
Pg/Lg Ratio
Frequency (Hz)
−116˚30' −116˚00'
37˚30'
37˚00'
36˚30'
km
0 10 20

Figure 9. Comparison of pairs of events at common subsets of stations. (a) Mean Pg/Lg ratios from SPE-4Prime and SPE-6 and map of stations that are used in the mean calculation. (b) Mean ratios and stations from DAG-1 and DAG-4. (c) Mean ratios and stations from LSECE-2 and DAG-1. In each case the yellow diamonds represent the shallower of the two events and the purple diamonds represent the deeper event. Error bars represent one standard deviation. Gray-shaded areas cover frequencies for which all stations are common for both events.

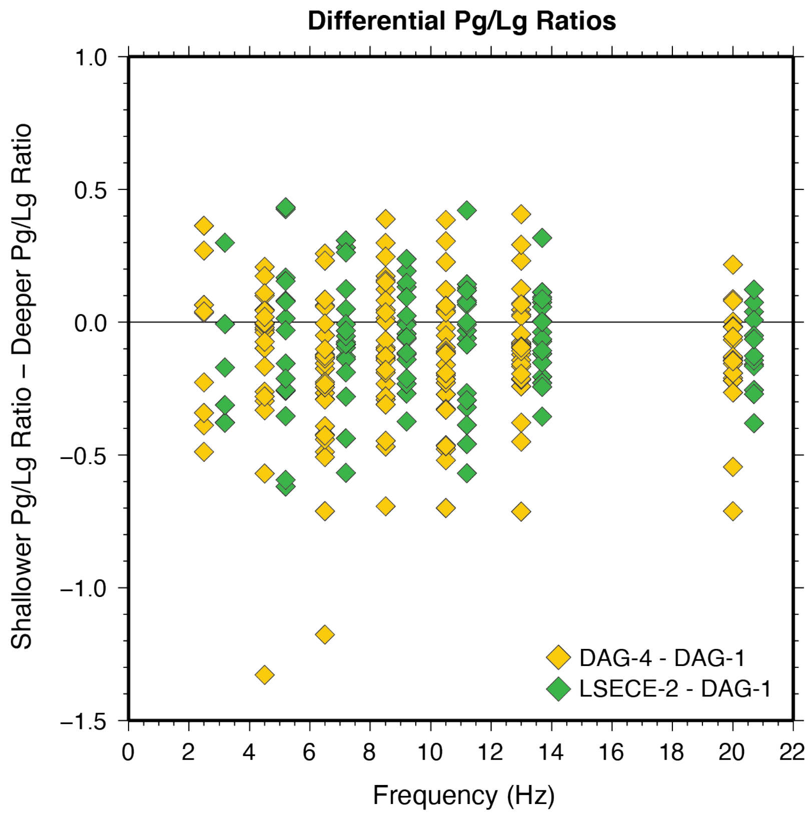

Figure 10. Differential Pg/Lg ratios for DAG-4 and DAG-1 (yellow diamonds) and LSECE-2 and DAG-1 (green diamonds).